

# Toward Safe Human–Robot Interaction: A Fast-Response Admittance Control Method for Series Elastic Actuator

Haoran Zhong, *Student Member, IEEE*, Xinyu Li<sup>ID</sup>, *Member, IEEE*,  
Liang Gao<sup>ID</sup>, *Senior Member, IEEE*, and Congbo Li<sup>ID</sup>, *Senior Member, IEEE*

**Abstract**—Series elastic actuator (SEA) is a promising compliance device due to its lower output mechanical impedance, and it is widely applied to ensure safe human–robot interaction. Although some efforts have been made to achieve accurate stiffness tracking, the time-delay issue in SEA control has still not been well investigated. However, the time delay can cause an inaccurate response and increase the risk of injury. To overcome this problem, this article proposes a fast-response admittance control method for SEAs. First, an admittance control scheme considering the external force estimation is developed for a hydraulic SEA. Then, a parallel adaptive time-series (ATS) (P-ATS) compensator is proposed and further adopted in the admittance control scheme to compensate for the time delay and tracking error. The P-ATS compensator is a modification of the ATS compensator, which is enhanced with a unique parallel mechanism. Such a mechanism can save more computational resources on locating better parameters for P-ATS compensator, thus improving its performance. Moreover, the parameter setting is converted to an optimization task, which is solved by the whale swarm algorithm (WSA) to achieve higher accuracy. The newly located parameters are compared to the current parameters based on a proposed evaluation criterion, thus guaranteeing the quality of the updated parameters. All the above strategies are employed to improve the SEA admittance control performance. The results obtained from both simulation and real-world experiments validate that, compared to conventional methods, the proposed method achieves a better performance in SEA stiffness tracking with lower time delay and tracking error.

**Note to Practitioners**—Accurate stiffness tracking of SEAs can achieve safe human–robot interaction. However, the time delays introduced by the imprecise movement and estimation of external force can lead to inaccurate actuator response that

Manuscript received November 22, 2020; revised January 16, 2021; accepted February 2, 2021. This article was recommended for publication by Associate Editor C.-Y. Lee and Editor C. Seatzu upon evaluation of the reviewers' comments. This work was supported in part by the National Key Research and Development Program of China under Grant 2018AAA0101704, in part by the National Natural Science Foundation of China under Grant 51721092, and in part by the Program for the HUST Academic Frontier Youth Team under Grant 2017QYTD04. (*Corresponding author: Liang Gao*)

Haoran Zhong, Xinyu Li, and Liang Gao are with the State Key Laboratory of Digital Manufacturing Equipment and Technology, School of Mechanical Science and Engineering, Huazhong University of Science and Technology, Wuhan 430074, China (e-mail: 1520098925@qq.com; lixinyu@hust.edu.cn; gaoliang@mail.hust.edu.cn).

Congbo Li is with the State Key Laboratory of Mechanical Transmission, Chongqing University, Chongqing 400030, China (e-mail: congibili@cqu.edu.cn).

Color versions of one or more figures in this article are available at <https://doi.org/10.1109/TASE.2021.3057883>.

Digital Object Identifier 10.1109/TASE.2021.3057883

may limit the capacity of safety insurance. To overcome this issue, a fast-response admittance control method is proposed for SEAs by adopting a novel P-ATS compensator. Thus, the time delays and errors from both load movement and external force estimation can be adaptively compensated. Several strategies have been adopted to enhance the compensator for parameter determination to achieve better performance. The proposed method requires no additional previous information about the system except load mass and spring stiffness, which makes it easy to implement for different types of SEAs. Experimental results show that the proposed method can achieve faster and more accurate stiffness tracking under different conditions. Future work aims to address the control problem under random disturbances and apply the proposed method to human–robot collaboration tasks to further test its performance.

**Index Terms**—Admittance control, delay compensation, manufacturing automation, series elastic actuator (SEA).

## I. INTRODUCTION

THE modern manufacturing industry is now shifting toward the production of small batches that require the robots and human workers to share their skills and workspace [1], [2]. In this case, collaborative robotic solutions have become the new frontier in the manufacturing industry [3]. The safety issue is a primary challenge especially in applications where close human–robot interaction is required [3], [4]. Traditional rigid robots are, therefore, less qualified due to the lack of versatility and flexibility [5], [6].

Thus, compliance techniques have been proposed to address these issues. In particular, series elastic actuators (SEAs) are considered as promising solutions for achieving interaction safety and high-performance control [7]–[12]. SEAs can ensure inherent compliance by introducing a flexible component, for example, spring, between the actuator and load [13]. Such a unique structure provides advantages, such as shock absorption, lower mechanical impedance, and energy storage [10], [14]–[17]. By combining the advantages of high precision and repeatability with flexibility and versatility, the SEAs allow human workers and robots to share the same space and collaboratively accomplish delicate manufacturing tasks. Recently, SEAs have been successfully applied to different industrial robots, such as IIWA [18] and Baxter [19]. They have also been employed in energy-efficient devices, exoskeletons, and rehabilitation robots [20]–[24].

Most studies on SEA have mainly focused on motor-based electric SEAs, with hydraulic SEAs receiving less attention. The major difference between motor and the hydraulic actuator is that the former one is regarded as a drivable actuator, while the latter one is generally considered as a rigid actuator with nonbackdrivability [25]–[27]. However, with the introduced elastic component, the hydraulic SEA allows a combination of high power-to-weight ratio with guaranteed interaction stability [27], [28]. Previous studies have validated the applicability and availability of hydraulic SEA in realizing safe human–robot collaboration tasks [29], [30].

Various control methods have been proposed for SEAs to realize active compliance. Calanca *et al.* [13] divided these techniques into three types: impedance control, admittance control, and direct force control. Compared to direct force control, impedance and admittance methods are designed to shape the impedance or admittance of robots under both contact and noncontact conditions; therefore, they are suitable for unknown environments [14], [31]–[33]. The difference between these two approaches is that the impedance control uses an inner force control loop, whereas the admittance control contains an inner position or velocity control loop [34]. Naturally, the latter one is more suitable for hydraulic SEA due to the nonbackdrivability of the hydraulic actuator [25]. However, the encountering problems for both types of SEAs are similar from the perspective of compliant control. In early studies, proportional–integral–derivative (PID)-based methods were widely applied to realize impedance or admittance control. Pratt *et al.* [35] and Robinson and Pratt [36] proposed a PID-based impedance controller to achieve a spring-like operation and applied it to control a biometric joint. Vallery *et al.* [37] developed an admittance control scheme to achieve stable torque tracking with the discussion of passivity and limitations. Although PID-based methods are considered to be simple and effective, they also suffer from inaccuracy and disturbance [28], [38], [39]. In fact, for a certain movement, learning-based methods can effectively improve tracking accuracy. Banka *et al.* [39] implemented an iterative machine learning (IML) method for high-precision position control of a robotic arm with unknown dynamics. However, the rejection of unknown disturbances remains a challenging issue. In recent years, disturbance observer (DOB) has attracted extensive interest to cope with the instability and inaccuracy caused by external disturbances and uncertainties [15], [40]–[42]. Oh and Kong [43] combined DOB with a feedback compensator to compensate for disturbance and tracking error. Most of the aforementioned methods assume that the external force is known, but an accurate estimation can be a challenge in real cases. A common and simple strategy is to measure the external force through the spring deflection [44]. However, the influence of load dynamics is nonnegligible, and it can introduce considerable errors [14], [44]. To address this problem, a machine learning-based technique was implemented for robotic manipulators without an accurate dynamic model [45]. Park *et al.* [14] designed an external force observer (EFO) for SEAs based on an inverse dynamic model.

Although many studies have been proposed to improve the control performance, the time-delay issue in SEA control

remains an unsolved problem. Time delay can be introduced by the use of filters and inaccurate actuator response, which exists in most SEA control systems [45]–[47]. For example, considerable delays are observed in external force estimation due to the low-pass filters that are used to eliminate high-frequency noise [14], [45]. Time delay causes a phase shift that leads to tracking errors and potential instability, resulting in notable performance losses [14], [47]–[49]. In addition, a small time delay can introduce significant stiffness variations under the contact condition, thereby increasing the risk of injury when interacting with humans [50], [51]. To overcome this problem, some delay-compensation methods have been proposed. The Smith predictor was developed to eliminate the SEA position drift of a haptic teleoperation system [52]. However, that study simply considers the condition of known constant delay. To cope with time-varying delay, Souzanchi-K *et al.* [48] considered the time delay as part of the uncertainties, which were further handled as external load dynamics. Although it can reduce the computational burden, such a method is unsuitable for systems with large delays. Kim and Bae [21] proposed a model-inverse time delay control (MiTDC) method for SEA force control in the application to a lower extremity exoskeleton system. The delay and disturbances can be canceled via a virtual reference obtained by the inverse model. Another effective model-based method was proposed by Phillips and Spencer [47], which converts the actuator tracking problem to a regulator problem of minimizing the time delay and tracking error. A feed-forward controller is also employed to cancel the hydraulic dynamics based on the inverse model. Even though most of the aforementioned methods have proven to be effective, the requirement of prior system information limits their practical application. Chae *et al.* [46], therefore, proposed an adaptive time-series (ATS) compensator for hydraulic SEAs, which can be implemented without knowing any previous information about the system. Although our previous work has validated its effectiveness in both error and delay compensation, simulation results also suggest that the compensator performance is easily affected by the sampling procedure [53].

To realize a fast and accurate response of stiffness tracking for SEAs, this article proposes a fast-response admittance control method that only requires the information of load mass and spring stiffness. The stiffness tracking can be easily achieved through the combination of a previously developed position controller and EFO [14], [54]. However, different from most current studies that mainly focus on SEA control rather than external force estimation [25]–[27], [46], [51], [54], this study presents a parallel ATS (P-ATS) compensator and further adopts it to both the SEA position controller and EFO, therefore improving the overall control performance in terms of delay and error reduction. The P-ATS compensator is an improved version of the ATS compensator with a unique parallel mechanism to enhance its performance while maintaining the advantage of ease of use. The parallel mechanism allows the data updating and parameter determination procedures to be conducted independently, thus saving more computational resources to locate better parameters. Especially, the determination of parameters in the P-ATS compensator is

transformed to a parameter optimization task, which is solved by the whale swarm algorithm (WSA) [55], [56]. Previous tests have confirmed the higher efficiency and afforded robustness of the WSA, which makes it suitable for this optimization task. In addition, an evaluation criterion is proposed to assess the quality of the identified parameters before updating, thus improving the parameter behavior and system stability. Finally, several simulation and real-world experiments were performed to validate the performance of the proposed control method.

The contributions of this article are summarized as follows.

- 1) The proposed method considers the time delays and errors in both the actuator response and external force estimation, which improves the overall performance.
- 2) Through the unique parallel mechanism and WSA method, the proposed P-ATS compensator improves the searching ability for parameter determination.
- 3) A higher quality of the updated parameters can be guaranteed with the evaluation criterion.
- 4) The influence of sampling rate is evaluated for the guidance to applications.

The remainder of this article is organized as follows. The admittance control scheme and problem description are presented in Section II. The P-ATS compensator is proposed and applied to develop the fast-response admittance control method in Section III. Simulation and real-world experiments are conducted to verify the proposals in Section IV. Finally, the conclusion and future work are provided in Section V.

## II. DEVELOPMENT OF ADMITTANCE CONTROL SCHEME AND PROBLEM DESCRIPTION

In this section, an admittance control scheme is designed based on the load dynamics of a hydraulic SEA to realize a fast-response stiffness tracking. First, the dynamic model of the presented SEA is constructed. Second, the holistic admittance controller is developed, in which an EFO is also introduced to estimate the external force. Finally, the time delay issue in the admittance controller is discussed.

### A. Development and Modeling of Hydraulic SEA

The developed hydraulic SEA is illustrated in Fig. 1(a), and Fig. 1(b) presents its schematic structure. According to the figures, the load movement can be controlled through the cylinder. The hydraulic SEA system can be divided into two parts: 1) hydraulic part, from control signal  $I$  (current) to cylinder extension  $D_a$  and 2) load part from  $D_a$  to load position  $D_l$ .

It should be pointed out that this SEA is developed as an experimental platform to validate the proposed control method. The SEA prototype designed for robotic manipulators has a similar but much smaller structure, as shown in Fig. 2. These two actuators are suggested to have the same dynamic characteristics.

The hydraulic dynamics are modeled based on the cylinder extension movement (positive to the right), in which the nonlinear parts are neglected. Therefore, the dynamic model of the valve-controlled asymmetric cylinder system

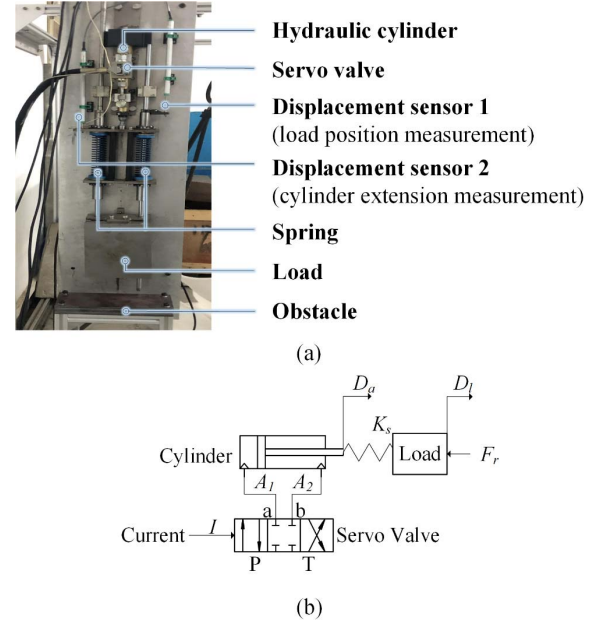


Fig. 1. Developed hydraulic SEA. (a) Hydraulic SEA system. (b) Schematic structure.

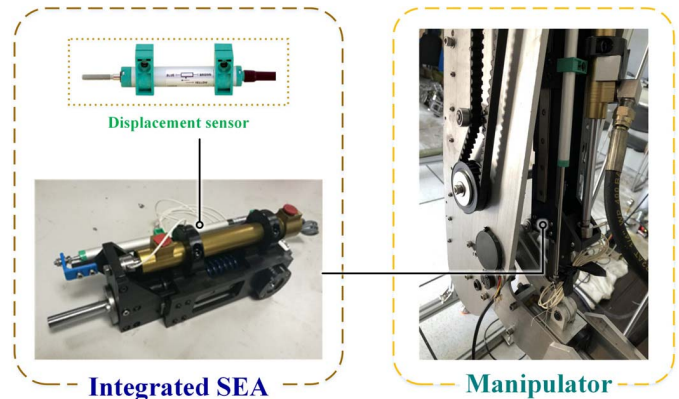


Fig. 2. SEA prototype designed for robotic manipulators.

$P_h(s) = D_a/I$  can be approximated as follows [57]:

$$D_a = \frac{K_v \frac{I}{A_1} - \frac{F}{A_1^2} \left[ K_{ce} + \frac{V_t}{2(1+n^2)\beta_e} s \right]}{s \left( \frac{s^2}{\omega_h^2} + \frac{2\varepsilon_h}{\omega_h} s + 1 \right)} \quad (1)$$

where

$$\omega_h = \sqrt{\frac{2(1+n^2)\beta_e A_1^2}{V_t M_L}}. \quad (2)$$

The definitions of the hydraulic coefficients and their values are presented in Table I. The hydraulic model is used for the experiment, whereas the proposed controller does not require information about hydraulic dynamics.

The load-side dynamics represent the relationship between the cylinder extension  $D_a$  and the load position  $D_l$ . According to Fig. 2, the dynamics can be described as follows:

$$F_r - (D_a - D_l)K_s + M_l \frac{d^2 D_l}{dt^2} = 0 \quad (3)$$

TABLE I  
HYDRAULIC PARAMETERS

Notation	Definition	Value	Notation	Definition	Value
$A_l$	Area of the rodless chamber	$2.01 \times 10^{-4} \text{ m}^2$	$V_t$	Cylinder volume	$1.96 \times 10^{-5} \text{ m}^3$
$A_2$	Area of the rod chamber	$8.80 \times 10^{-5} \text{ m}^2$	$N$	$A_2/a_l$	0.44
$K_v$	Current flow gain of valve	$1.15 \times 10^{-2} \text{ m}^3/(\text{s}\cdot\text{a})$	$M_l$	Load mass	15 Kg
$K_{ce}$	Flow pressure coefficient	$1.24 \times 10^{-13}$	$E_h$	Damping coefficient	0.15
$\beta_e$	Density of hydraulic fluid	$1.30 \times 10^9 \text{ pa}$	$F$	Load force	—
$P_s$	System pressure	21 MPa	$Q_s$	System flow rate	11 L/min
$K_s$	Spring stiffness	2700 N/m	$P_s$	System power	4 kW

where  $F_r$  and  $M_L$  denote the external force and load mass, respectively, and  $K_s$  represents the equivalent stiffness of the two springs. The friction within the hydraulic system is neglected due to the nonsensitivity in position control [7]. Therefore, the nominal load-side dynamic model  $P_{ln}(s) = D_l/D_a$  can be derived through the Laplace transform as follows:

$$D_l = \frac{D_a K_s - F_r}{M_l s^2 + K_s}. \quad (4)$$

### B. Proposed Admittance Control Scheme

In this section, we propose an admittance control method based on the nominal model  $P_{ln}(s)$ . We have previously developed a high-precision position controller using DOB [54]. It handles the tracking error introduced by the cylinder extension control and hydraulic model uncertainties as the disturbance, which can be suppressed by the DOB. The feedback compensator is also combined to improve the tracking accuracy. In this study, we adopt an outer admittance control loop to shape the contact impedance by computing a position variation  $\Delta l$  according to the external force,  $F_r$ , and, therefore, realize the admittance control. The admittance model  $P_k(s)$  can be represented as follows:

$$P_k(s) = \frac{\Delta l}{F_r} = \frac{1}{D_d s + K_d} \quad (5)$$

where  $D_d$  and  $K_d$  represent the desired damping and stiffness, respectively. Fig. 3 presents the holistic admittance control scheme, in which the inner load position control loop contains three parts: a DOB, a cylinder control loop, and a feedback compensation loop.

The cylinder movement is formed as an ideal position source by using a PID controller, and the tracking error and hydraulic model uncertainties are taken as the input disturbance of the load dynamics. The DOB was developed based on the inverse nominal model  $P_{ln}(s)$ .  $Q(s)$  represents a second-order Butterworth filter to make the inverse model realizable and

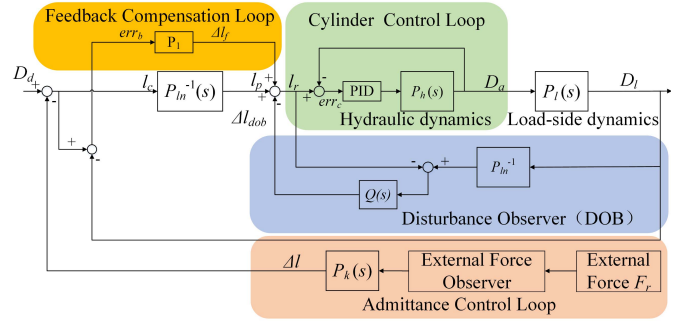


Fig. 3. Block diagram of the admittance control scheme.

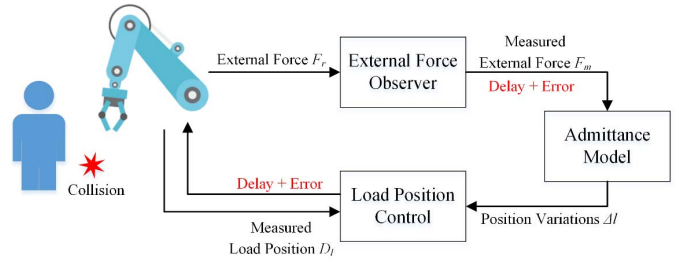


Fig. 4. Schematic of admittance control scheme with delay.

eliminate high-frequency noise, which takes the form of

$$Q(s) = \frac{1}{(s/\omega_f)^2 + \sqrt{2}(s/\omega_f) + 1} \quad (6)$$

where  $\omega$  represents the cutoff frequency, which is set to 15 Hz. The DOB is used to improve the system's robustness and suppress the disturbance. A feedback proportional controller  $P_1$  is also combined to compensate directly for the load tracking error.

In this study, an EFO is introduced to measure the external force  $F_r$ . In the EFO, proposed by Park *et al.* [14], the load dynamics are considered. Moreover, it requires no additional information about the system. The EFO is developed based on the inverse nominal model  $P_{ln}(s)$  as follows:

$$F_m = \frac{D_l(M_l s^2 + K_s)}{D_a K_s Q(s)} \quad (7)$$

where  $Q(s)$  represents the second-order Butterworth filter. A mean filter was also employed to obtain a smoother curve. The cutoff frequency in both filters was set at the same value of 15 Hz.

### C. Delay Issue Description

The proposed admittance control scheme allows the hydraulic SEA to track the desired stiffness and damping by adjusting the target load position according to the measured external force. Therefore, the admittance control performance depends on the accuracy of both the load position tracking and external force estimation. However, the load movement and EFO can introduce time delay and tracking error, which leads to significant performance losses, as shown in Fig. 4. In position control, the errors can be caused by inaccurate

actuator response due to the defects of controller and hardware limitations, such as valve flow. The errors in EFO, however, are mainly introduced by the use of the filters [46]. Furthermore, in real-world cases, the delay is usually time-varying, which makes it difficult to compensate by using traditional methods. Such influence not only adversely affects the SEA performance but also increases the risk of injury in human–robot interaction.

### III. PROPOSED FAST-RESPONSE ADMITTANCE CONTROL METHOD

In this study, we propose a novel P-ATS compensator to enhance the SEA control performance. Both time delay and tracking error can be compensated via a P-ATS compensator, thereby improving the overall control performance. In this section, the original ATS compensator is introduced. Second, the improved P-ATS is proposed and then employed in the proposed admittance control scheme to realize high-performance control. Finally, the influences of the sampling rate are discussed.

#### A. Introduction of ATS-Compensator

To achieve fast response, Chae *et al.* [46] proposed an ATS compensator for force control of a servo-hydraulic system. For each period, the ATS compensator updates the data set of measured values (i.e., sampling procedure) and the control parameters (i.e., parameter determination procedure) in sequence.

Provided that the actuator output,  $T_m$ , contains a time delay,  $\tau_p$ , and amplitude decay,  $L_p$ , the relationship between  $T_m$  and target input,  $T_d$ , at time  $k$  can be described as follows:

$$T_d = \frac{1}{L_p} T_m(k + \tau_p). \quad (8)$$

This equation can be approximated with the Taylor series

$$T_d = a_0 T_m + a_1 \dot{T}_m + \dots + a_n \frac{d^n T_m}{dt^n} \quad (9)$$

where

$$a_i = \frac{\tau^i}{L_p i!}, \quad i = 0, 1, \dots, n. \quad (10)$$

The maximum order is set to 2 ( $i = 2$ ). Therefore, to match the actual output ( $T_m$ ) with the target ( $T_d$ ), a set of parameters  $\mathbf{P} = [P_1, P_2, P_3]$  is used to compensate for the input. Therefore, the compensated input,  $T_c$ , at time  $k$  can be described as follows:

$$T_c^k = P_1^k T_d^k + P_2^k \dot{T}_d^k + P_3^k \ddot{T}_d^k \quad (11)$$

where  $T_d$  represents different types of signals, such as position or force. The parameter matrix  $\mathbf{P} = [P_1, P_2, P_3]$  can be determined by minimizing the following objective function:

$$\text{Fit} = \sum_{i=1}^j (T_c^{k-i} - T_e^{k-i}) \quad (12)$$

where  $j$  represents the sampling number. The values over a certain period  $j \Delta t$  ( $\Delta t$  represents the system sampling time) are restored in the data set for computation. During the

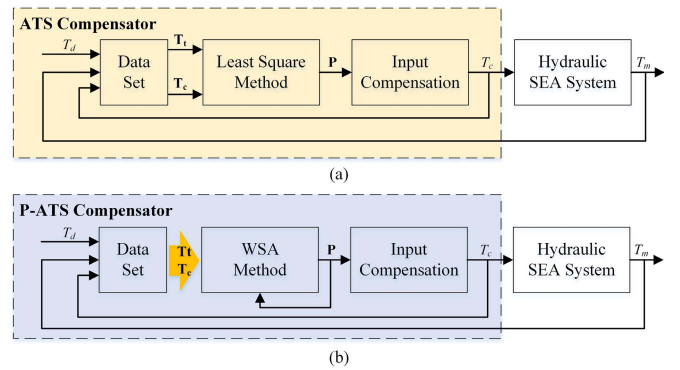


Fig. 5. Structures of ATS and P-ATS compensators. (a) ATS compensator, in which the data sampling and determination and updating of parameter matrix  $P$  are conducted in sequence for each period. (b) P-ATS compensator, in which the sampling procedure and parameter determination procedure are conducted independently, and the parameter matrix  $P$  can be updated only if a better solution has been found.

sampling procedure, the first value in the data set is replaced by the latest value for each sampling period.  $T_e$  represents the estimated compensated input, which can be written as follows:

$$T_e = P_1 T_m + P_2 \dot{T}_m + P_3 \ddot{T}_m \quad (13)$$

where  $T_m$  denotes the measured output. To match the actuator output,  $T_e$ , with the target input,  $T_d$ , the objective function value should be minimized. Thus, the parameter matrix  $\mathbf{P} = [P_1, P_2, P_3]$  can be obtained via the least-squares (LS) method as follows:

$$\mathbf{P}^T = (\mathbf{T}_t^T \mathbf{T}_t)^{-1} \mathbf{T}_t^T \mathbf{T}_c \quad (14)$$

where  $\mathbf{T}_t = [\mathbf{T}_m \dot{\mathbf{T}}_m \ddot{\mathbf{T}}_m]$ ,  $\mathbf{T}_m = [T_m^{k-1} \ T_m^{k-2} \ \dots \ T_m^{k-j}]^T$ , and  $\mathbf{T}_c = [T_c^{k-1} \ T_c^{k-2} \ \dots \ T_c^{k-j}]^T$ .

The LS-based ATS compensator updates the parameters based on historical data and does not require any previous system information. Such features make it an appropriate solution for improving the SEA control performance. The holistic structure of the ATS compensator is presented in Fig. 5(a). However, the ATS compensator has several limitations as follows.

- 1) The parameter determination procedure lacks a criterion to evaluate the parameter quality, resulting in inappropriate tuning that can cause instability.
- 2) The ATS compensator periodically updates the parameter matrix  $\mathbf{P}$ , while the computational resources between the sampling intervals are wasted.
- 3) The LS method is inefficient, which leads to inaccuracy.

#### B. Proposed P-ATS Compensator

In this section, we developed an improved P-ATS compensator with a parallel mechanism. The word “parallel” indicates that the parameter determination procedure is conducted in parallel to the sampling procedure (i.e., in the sampling procedure, the latest information is obtained to update the data set). Furthermore, the parameter determination task is converted to an optimization problem, which can be solved by using the WSA to determine appropriate parameters due to its good searching ability.

```

Input: The whale swarm  $\Omega$ , a whale  $\Omega_u$ .
Output: The “better and nearest” whale of  $\Omega_u$ .
begin
Define an integer variable  $v$  initialized with 0;
Define a float variable  $temp$  initialized with infinity;
for  $i=1$  to  $|\Omega|$  do
    if  $f(\Omega_i) < f(\Omega_u)$  then
        if  $dist(\Omega_i, \Omega_u) < temp$  then
             $v=i$ ;
             $temp=dist(\Omega_i, \Omega_u)$ ;
        end if
    end if
end for
return  $\Omega_v$ ;
end

```

Fig. 6. Pseudocode for finding “better and nearest” members.

In contrast to the ATS compensator, the P-ATS compensator independently updates the data set and control parameters. The modified parallel mechanism can be described as follows.

- 1) The sampling procedure periodically updates the data set, which remains unchanged with that in the ATS compensator.
- 2) A fitness function is taken as the criterion to evaluate the parameter quality, which is developed based on (12).
- 3) The parameter determination procedure uses the WSA algorithm to continuously optimize the coefficient matrix  $\mathbf{P}$ . The newly generated  $\mathbf{P}^*$  needs to be evaluated via the evaluation criteria. The output  $\mathbf{P}$  can be updated only if  $\mathbf{P}^*$  is better. Otherwise,  $\mathbf{P}$  remains unchanged.

The proposed unique parallel mechanism allows the updating of the data set and the parameter determination to be conducted independently. In this case, the optimization procedure can be continuously performed during the entire movement regardless of the sampling procedure. Therefore, compared with the ATS compensator, the P-ATS compensator can make full use of the computational resources between sampling intervals and optimize the parameters via WSA for various iterations. Furthermore, unlike the ATS compensator, the new matrix  $\mathbf{P}^*$  generated by WSA cannot directly update the current matrix  $\mathbf{P}$ . The P-ATS compensator provides a criterion to evaluate the quality of the current and newly determined parameter matrices. It will first compare their fitness values and then select the best solution. This evaluation process can improve the quality of output parameters and suppress the noise introduced by inappropriate parameter tuning.

The WSA is a powerful metaheuristic algorithm proposed for solving optimization problems. Previous studies have proven its superiority over conventional algorithms in terms of both searching ability and stability [55], [56], which makes it appropriate for this parameter optimization task. The WSA has a unique evolution mechanism that allows the search agents to follow the lead of their corresponding “better and nearest” members. The “better and nearest” member  $Y$  of a certain agent  $X$  denotes that  $Y$  has better fitness value and stays closest to  $X$ . The pseudocode of finding “better and nearest” member is shown in Fig. 6. Thus,  $X$  can move to another potential position, which can be expressed as follows based

on recommendation:

$$X^* = X + \text{rand}(0, 2) * (Y - X) \quad (15)$$

where  $\text{rand}(0, 2)$  represents a random number in a 0–2 range that is uniformly distributed. The parameter is selected based on the recommendation from the corresponding reference [55]. The better member between  $X$  and  $X^*$  will be admitted to the next generation. For the agent  $X$  that locates in the current best position, there exists no corresponding “better and nearest” member; thus, a neighborhood search strategy is adopted to generate the new position for  $X$  as follows:

$$X^* = X + \text{rand}(0.5, 1) * (X_i - X_j) \quad (16)$$

where  $X_i$  and  $X_j$  represent the nearest members to  $X$ . The WSA-based parameter determination follows the following steps.

- 1) Initialize the population group. Each individual contains a 3-D vector that represents the parameter matrix  $\mathbf{P}$ .
- 2) Normalize each individual to the 0–1 range and input the population group to WSA.
- 3) Find the corresponding “better and nearest” member of each individual, and generate their competitors based on (15) and (16).
- 4) Restore all variables of each individual and its competitor to actual values and calculate fitness values based on (12). The better one is allowed for the next generation.
- 5) Compare each individual to the current optimum value and update the optimum value if better.
- 6) Update the current parameter matrix  $\mathbf{P}$  using the optimum value.
- 7) Return to step 2.

The holistic structure of the P-ATS compensator is presented in Fig. 5(b).

### C. Development of Fast-Response Admittance Control Method

As described before, the time delay is mainly introduced by load position control and external force estimation. Thus, we employ the P-ATS compensators to these two loops and develop a fast-response admittance control method.

The P-ATS compensator can be directly applied to the SEA position controller, that is, a P-ATS-based position controller. The compensated target input,  $d_c$ , is determined by using the target input  $D_d$  and parameter matrix  $\mathbf{P}_d = [P_{d1}, P_{d2}, P_{d3}]$  as follows:

$$D_c = P_{d1}D_d + P_{d2}\dot{D}_d + P_{d3}\ddot{D}_d. \quad (17)$$

The parameter matrix  $\mathbf{P}_d$  can be obtained by using the WSA to minimize the following fitness function:

$$\text{Fit}_p = \sum_{i=1}^j (D_c^{k-i} - D_e^{k-i}) \quad (18)$$

where  $D_e$  represents the measured compensated target position, which can be written as follows:

$$D_e = P_{d1}D_l + P_{d2}\dot{D}_l + P_{d3}\ddot{D}_l \quad (19)$$

where  $D_l$  denotes the measured load position.

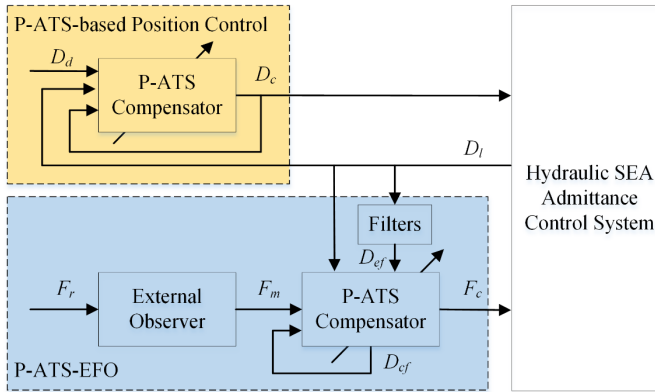


Fig. 7. Schematic of the proposed fast-response admittance control method.

An improved EFO with P-ATS compensator, that is, P-ATS-EFO, is also developed in this section. Unlike load position control, the P-ATS compensator, however, cannot be directly applied to EFO because there exists no target signal (i.e., actual force is unknown). In fact, it is not a control problem. The discussion in the previous section suggests that the delays and estimation errors are mainly introduced by the filter. Therefore, we select the load position,  $D_l$ , as the reference target input, and further input  $D_l$  to the same filters as used for EFO to obtain the reference output  $D_{ef}$ . Therefore, the control parameters for P-ATS-EFO are determined based on the reference signals. The reason for this selection is that: 1)  $D_l$  can be easily obtained; 2) no additional variables are introduced; and 3) according to (7),  $D_l$  is a major variable to obtain the estimated force. Therefore, an improved EFO with a P-ATS compensator was developed.

Similarly, the compensated external force,  $F_c$ , is determined as follows:

$$F_c = P_{f1}F_m + P_{f2}\dot{F}_m + P_{f3}\ddot{F}_m \quad (20)$$

where  $P_{f1}$ ,  $P_{f2}$ , and  $P_{f3}$  are the control parameters of the P-ATS compensator, and  $F_m$  represents the noncompensated force obtained by the EFO. The parameter matrix  $\mathbf{P}_f = [P_{f1}, P_{f2}, P_{f3}]$  can be determined using the reference data to minimize the following fitness function:

$$\text{Fit}_f = \sum_{i=1}^j (D_{cf}^{k-i} - D_{ef}^{k-i}) \quad (21)$$

where  $D_{cf}$  and  $D_{ef}$  represent the reference compensated input and measured compensated input, respectively.  $D_{cf}$  is determined as follows:

$$D_{cf} = P_{f1}D_l + P_{f2}\dot{D}_l + P_{f3}\ddot{D}_l \quad (22)$$

where  $D_{ef}$  can be written as follows:

$$D_{ef} = P_{f1}D_l + P_{f2}\dot{D}_l + P_{f3}\ddot{D}_l. \quad (23)$$

The proposed fast-response admittance control method is, therefore, developed with the structure presented in Fig. 7.

#### D. Discussion of Sampling Rate Influence

An important coefficient in ATS and P-ATS compensators is the sample size of the data set that restores the historical information (e.g.,  $T_m$  and  $T_e$  in ATS compensator). Smaller sample size can degrade the quality of determined parameters and, therefore, adversely affect the control performance. The sample size is determined by the sampling time period and the sampling rate. Normally, the time period is set to 1 s, indicating that we focus on the historical information in the latest 1 s [44]. Thus, a certain sample rate  $f_s$  generates a sample size of  $f_s$ .

However, regardless of how large the sampling rate is, the ATS-compensator can only optimize the parameter once in each time period because the procedures of sampling and parameter determination are mutually affected. Thus, the performance can be severely affected by the reduction in the sampling rate. Although a higher sampling rate can benefit the process, it increases the computational burden, without obtaining a guarantee of finding a better solution. In previous works [46], [51], the influences of such important coefficients were not discussed. Thus, the selection of an appropriate sampling rate with hardware limitations remains a challenge. In addition, a fixed updating period makes the procedure sensible to disturbances, such as transmission delay, since the ATS compensator needs to update the parameter periodically with limited time.

The P-ATS compensator aims to overcome this issue with the parallel mechanism. The unique mechanism allows the procedures of sampling and parameter determination to be conducted independently. In this case, the P-ATS compensator can continuously optimize the parameters without a time limit. The quality of the determined parameter is guaranteed with the evaluation criterion and more optimization generations, thereby compensating for the influence of sampling rate reduction. Such features also allow the P-ATS compensator to work effectively under conditions of variable sampling rate, thus facilitating its practical application. The influences of reducing the sampling rate are evaluated in the next section.

## IV. EXPERIMENTAL RESULTS AND DISCUSSION

In this section, the simulation and real-world experiments are performed to validate the effectiveness of the proposed method in reducing time delay and tracking error for SEA. Two methods are selected for comparison: 1) ATS-based method and 2) noncompensated method. First, we conduct the simulation experiments to evaluate the general performance; then, we apply the proposed method to the presented experimental platform to test the practical performance.

#### A. Experimental Setup

For simulation experiments, the platform is constructed in MATLAB 2017b/Simulink software with a system step time  $\Delta t = 0.001$  s (1000 Hz). The specifications of the hydraulic dynamics are provided in Section II. The following experiments are implemented.

##### 1) Experiment 1 (Variable Stiffness Tracking Experiment):

The external force is set to a constant value of 200 N,

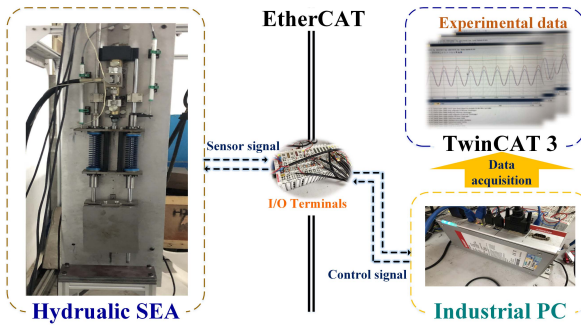


Fig. 8. Structure of the experimental platform.

whereas a 5-Hz sine wave with a form of  $5000 + 1000 \sin(10\pi t)$  is selected as the target stiffness. The sampling rate is set to 100 Hz.

- 2) *Experiment 2 (Collision Experiment):* The target stiffness is set to a constant value of 5000 N/m, whereas a 5-Hz sine wave with a form of  $200s \sin(10\pi t)$  is selected as the external force. The sampling rate is set to 100 Hz.
- 3) *Experiment 3 (Variable Sampling Rate Experiment):* Performances of variable stiffness tracking with both 50- and 20-Hz sampling rates are evaluated.

Experiment 1 is designed to verify the performance of the P-ATS-based position controller in dynamic stiffness tracking. Experiment 2 assesses the SEA performance under the disturbances of varying external forces. In Experiment 3, the influences of the sampling rate are evaluated. In this study, we aim to focus on the stiffness rather than damping since the former plays a more important role in ensuring safe human–robot interaction [58]. Thus, the damping coefficient is set to zero to realize pure stiffness tracking.

For real-world experiments, the control system consists of an industrial computer (Beckhoff, C6920-0050) and input–output terminals quipped with a TwinCAT 3 software system. The cylinder extension and load movement can be measured through two displacement sensors. The structure of the experimental platform is shown in Fig. 8. The variable stiffness tracking and collision experiments (i.e., Experiment 1 and 2) are conducted.

Different from that, in the simulation experiments, in the collision experiment, we control the SEA to hit the obstacle instead of applying a certain varying external force on the load.

Therefore, by using different methods, the estimated contact forces are mutually different, due to the diverse control performance. When the collision happens, the velocity of the SEA load is equal to zero. In this case, the actual contact force can be measured through spring deflection directly. For safety concerns, we take the optimized parameters obtained from simulation experiments for the initial parameters in the real-world cases.

For each experiment, time delays at the 10th peak,  $\tau^{10}$ , and the 30th peak,  $\tau^{30}$ , are selected. The reason for such selection is that we aim to evaluate both the short-and long-term effectiveness of the competitive methods. Moreover, in our case, we hope that the SEA can realize a fast-response tracking

TABLE II  
CONTROL PARAMETERS

Control parameter	Definition	Value
$K_p$	Proportional gain of PID controller	1.2
$K_i$	Integral gain of PID controller	0.1
$P_1$	Proportional gain of P1	0.01

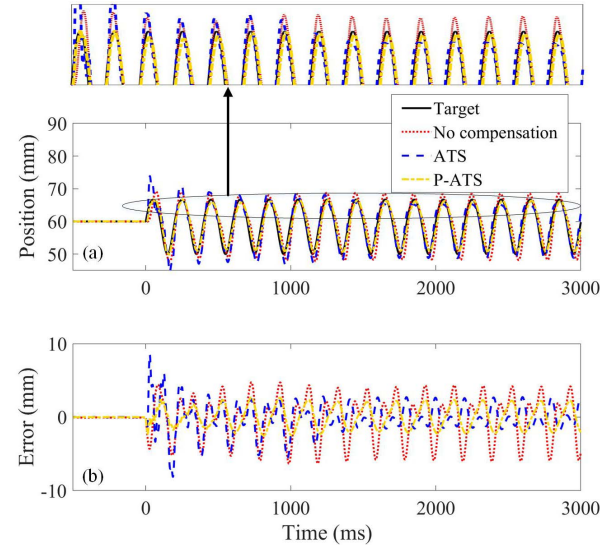


Fig. 9. SEA response performance. (a) Load position. (b) Tracking error.

in less than 1 s. Other performance indexes, such as maximum,  $e_{k \max}$ , and average stiffness tracking,  $e_k$ , are also selected to draw a more quantitative conclusion. The specific indexes are introduced in the corresponding experiments.

The specifications of hydraulic dynamics are provided in Section II, whereas the control parameters are listed in Table II. The values are chosen to be consistent with the developed hydraulic SEA system. In WSA, the population size and the maximum number of the iterative counter are set to 30 and 50, respectively [55]. The simulation experiments aim to evaluate the compensator response to a dynamic environment rather than simply obtain a high-performance result. Thus, the parameter matrices  $\mathbf{P}$ ,  $\mathbf{P}_d$ , and  $\mathbf{P}_f$  in both P-ATS and ATS compensators are set to  $[1, 0, 0]$  at first, respectively, indicating no compensation signal. Based on recommendation [46], the ranges of all coefficient matrices for each row are set to  $(0.1, 2)$ ,  $(0, 0.1)$ , and  $(0, 0.005)$ , respectively. To eliminate the randomness of the WSA method, each experiment is independently conducted three times to obtain average results.

### B. Variable Stiffness Tracking Experiment

Fig. 9 shows the results of SEA response (i.e., load position tracking) when target stiffness is variant. The parameter variations of P-ATS and ATS compensators in the SEA position controller are shown in Fig. 10. In Fig. 11, the results of the variable stiffness tracking experiment are presented.

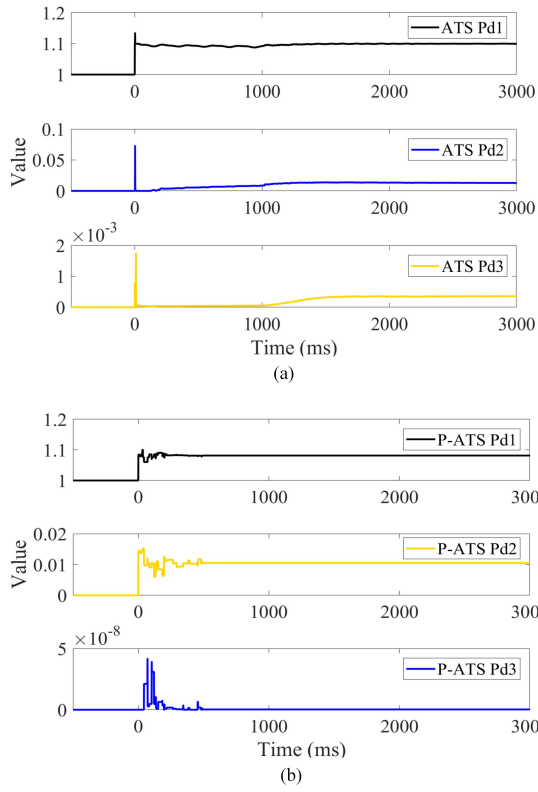


Fig. 10. Parameter variations in the SEA position controller. (a) ATS compensator. (b) P-ATS compensator.

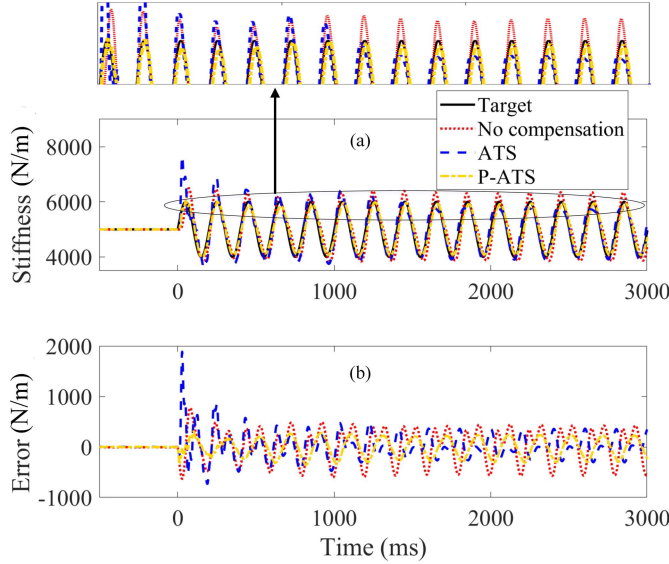


Fig. 11. Variable stiffness tracking performance. (a) SEA stiffness. (b) Tracking error.

As can be observed in Fig. 9, compared with the comparative methods, the P-ATS-based method performs the best with an almost negligible time delay and tracking error. The ATS-based method, however, has the largest overshoot at the beginning and converges to the desired position much slower, whereas the noncompensated method presents an obvious tracking error during the entire movement. From Fig. 10(a), a severe vibration is observed at the initial stage, and each

TABLE III  
VARIABLE STIFFNESS TRACKING RESULTS

Method	$\tau_d^{10}$ [ms]	$\tau_d^{30}$ [ms]	$e_{\text{dmax}}$ [mm]	$e_d$ [mm]	$v_d$	$e_{k\text{max}}$ [N/m]	$e_k$ [N/m]
NC	22	19	6.3	2.1	---	774.2	241.4
ATS	13	-3	8.6	1.5	11.7	1887.5	190.5
P-ATS	8	5	2.6	1.2	1.6	354.1	157.9

\*NC: non-compensated method. Negative value indicates a phase advance.

parameter continuously fluctuates around an equilibrium position after 1000 ms. This explains the reason for the larger overshoot and convergence time. In Fig. 10(b), the parameter variations in the P-ATS compensator remain unchanged after 500 ms, indicating that no better solutions are found. The results of variable stiffness tracking in Fig. 11 are consistent with those of actuator response.

In this experiment, seven performance indexes are provided, that is, delay at the 10th peak  $\tau_d^{10}$ , delay at the 30th peak  $\tau_d^{30}$ , maximum response error  $e_f^{\text{max}}$ , average response error  $e_f$ , average fitness value  $v_d$ , maximum stiffness tracking error  $e_{k\text{max}}$ , and average stiffness tracking error  $e_k$ . The results are summarized in Table III. In this study, phase advance is considered as an error introduced by overcompensation. It can be observed that, compared with the ATS-based method, although the ATS compensator shows slightly better performance in the long term (5 compared to -3 ms), the P-ATS compensator has a faster response at the early stage (8 compared to 13 ms). In addition, the results suggest that the P-ATS compensator achieves a 20% (from 1.5 to 1.2 mm) and a 17.1% (from 190.5 to 157.9 N/m) improvements in average position and stiffness tracking errors, respectively, which is consistent with the results of fitness values. The proposed method clearly shows better tracking performance in this experiment.

*Remark 1:* Both ATS and P-ATS compensators can effectively reduce the tracking error and time delay, thus providing a more accurate actuator response. However, the ATS compensator achieves a worse performance due to the inappropriate parameters. In contrast, in the P-ATS compensator, the parallel mechanism aids in providing more computational resources for optimizing the parameters, thus increasing the chance of finding a better solution. In addition, proven by the average fitness values, the WSA method has better searching ability than the LS method. Moreover, the introduced evaluation criterion enables the P-ATS compensator to output high-quality parameters and eliminate inappropriate and unnecessary tuning for parameters, thereby improving performance and avoiding instability when encountering a dynamic environment.

### C. Collision Experiment

Fig. 12 shows the results of external force estimation. The parameter variations of P-ATS and ATS compensators in EFO are shown in Fig. 13, and the results of actuator response and stiffness tracking are presented in Fig. 14.

It can be observed from Fig. 12(a) that both ATS-EFO and P-ATS EFO can rapidly react to the sudden change of external force. The curve obtained by P-ATS-EFO lies closer to the actual force. Supported by Fig. 12(b), the estimation error

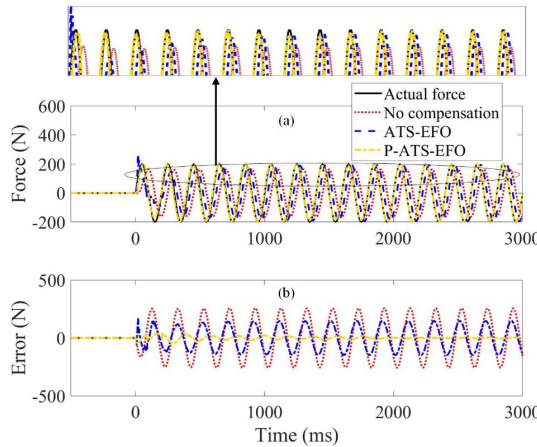


Fig. 12. External force estimation. (a) Force estimation results. (b) Estimation error.

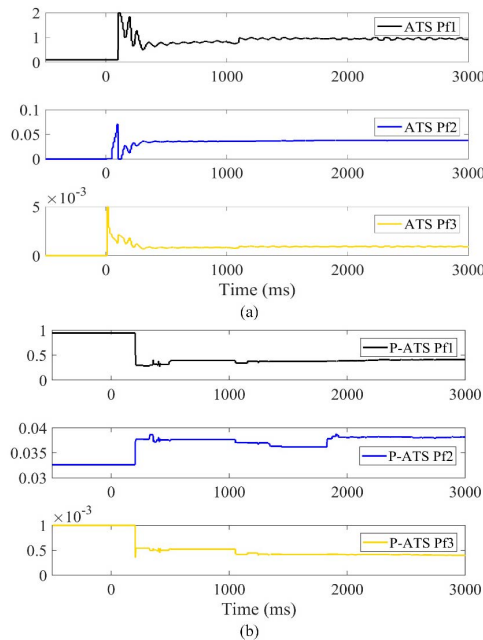


Fig. 13. Parameter variation in EFO. (a) ATS compensator. (b) P-ATS compensator.

obtained by P-ATS-EFO gradually converges to zero. Similar to that in Experiment 1, the ATS-EFO has a larger overshoot. Although the ATS-EFO can converge to a steady state in the second period, a constant time delay is observed. The non-compensated method, however, reacts much slower when the external force is applied, and a massive time delay and tracking error are introduced. According to Fig. 13, a more fluctuant curve is observed in the P-ATS compensator, especially at the initial stage. Fig. 14 shows the stiffness variations after the external force is applied. It is clear that, by using the P-ATS compensator, the SEA can main the desired stiffness under the disturbances introduced by the varying external force. The other two methods, however, obtain a larger error.

Accordingly, seven performance indexes are provided for further analysis, that is, delay at the 10th peak  $\tau_f^{10}$ , delay at

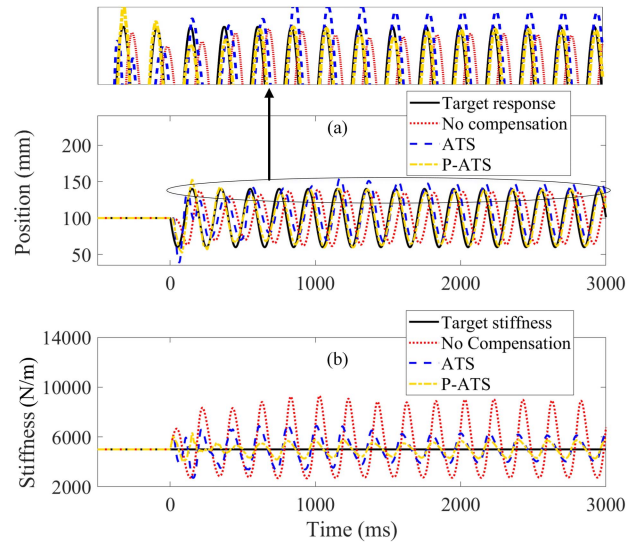


Fig. 14. Collision results. (a) Actuator response result. (b) Stiffness variations under disturbances of external force.

TABLE IV  
COLLISION RESULTS

Method	$\tau_f^{10}$ [ms]	$\tau_f^{30}$ [ms]	$e_{f\max}$ [N]	$e_f$ [N]	$v_f$	$e_{k\max}$ [N/m]	$e_k$ [N/m]
NC	51	50	257.4	156.0	---	4299.2	1589.8
ATS	25	25	165.5	89.0	0.13	2285.4	833.8
P-ATS	-3	-1	46.8	9.5	0.10	1312.8	404.5

\*NC: non-compensated method. Negative value indicates a phase advance.

the 30th peak  $\tau_f^{30}$ , maximum response error  $e_{f\max}$ , average response error  $e_f$ , average fitness value  $v_f$ , maximum stiffness error  $e_{k\max}$ , and average stiffness tracking error  $e_k$ . The results are summarized in Table IV. For all methods, the achieved time delays in the 10th peak are similar to that in the 30th peak, indicating that a fast convergence. However, with the P-ATS compensator, a much smaller delay in force estimation is achieved (25 compared to -1 at the 30th peak). Moreover, the proposed method aids in reducing 89.3% (from 89.0 to 9.5 N) of average force estimation error and 51.5% (from 833.8 to 404.5 N/m) average stiffness tracking error.

*Remark 2:* Compared with that in Experiment 1, the ATS compensator converges faster but also introduces a larger time delay, whereas the P-ATS compensator achieves similar results. Such performance is due to the filters used in EFO, which introduces a more significant delay than that in actuator response, therefore degrading the performance of the ATS compensator. However, the parallel mechanism allows a continuous optimization for the P-ATS compensator by using the WSA method. In this case, the P-ATS compensator is less affected by the enlarged delay. Also, for force estimation, the presence of time delay and tracking error in the reference signal is permanent and cannot be eliminated through the compensator. Such a feature not only makes it a different task in force estimation but also leads to faster convergence. In addition, the stiffness tracking performance in Experiment 2 is worse than that in Experiment 1. The reason is that,

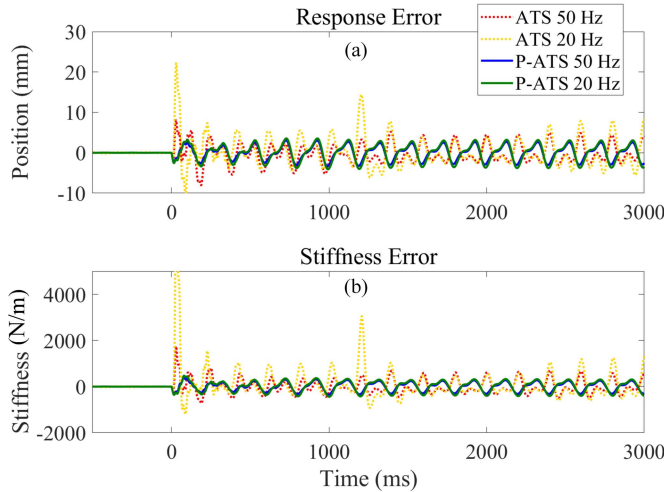


Fig. 15. Variable stiffness tracking performance with variable sampling rate. (a) Actuator response error. (b) Stiffness tracking error.

TABLE V  
STIFFNESS TRACKING RESULTS UNDER VARIABLE SAMPLING RATE

Method	$\tau_d^{10}$ [ms]	$\tau_d^{30}$ [ms]	$e_{dmax}$ [mm]	$e_d$ [mm]	$v_d$	$e_{kmax}$ [N/m]	$e_k$ [N/m]
ATS 50 Hz	12	-5	8.1	2.0	2.7	1748.5	247.8
ATS 20 Hz	6	-5	22.2	2.8	11.6	10487.2	422.4
P-ATS 50 Hz	10	8	3.3	1.4	1.1	414.3	167.8
P-ATS 20 Hz	14	8	4.1	1.8	1.3	473.4	203.6

\*Negative values indicate a phase advance.

in Experiment 2, the actuator performs a larger movement range, and the errors are derived from both the force estimation and actuator response.

#### D. Variable Sampling Rate Experiment

Fig. 15 shows the results of variable stiffness tracking with a variable sampling rate. As we can observe from the figure, the ATS compensator suffers significant performance losses from the reduced sampling rate. In particular, in the 20-Hz experiment, the ATS-based method performs worse than the noncompensated method, as shown in Experiment 1. Moreover, no obvious degradation is observed for the proposed method. Further details are summarized in Table V.

Based on the results from Table V, it can be observed that the ATS compensator tends to be more easily affected by the reduction in the sampling rate. The ATS compensator suffers a 40.0% (2.0–2.8 mm) and 70.5% (247.8–422.4 N/m) deterioration in average position and stiffness tracking errors. By comparison, the ATS compensator suffers a 28.6% (1.4–1.8 mm) and 21.3% (167.8–203.6 N/m) deterioration in the same two criteria, respectively. In terms of time delay, the ATS compensator achieves the best result under a 20-Hz sampling rate. However, other indexes and results from Fig. 15

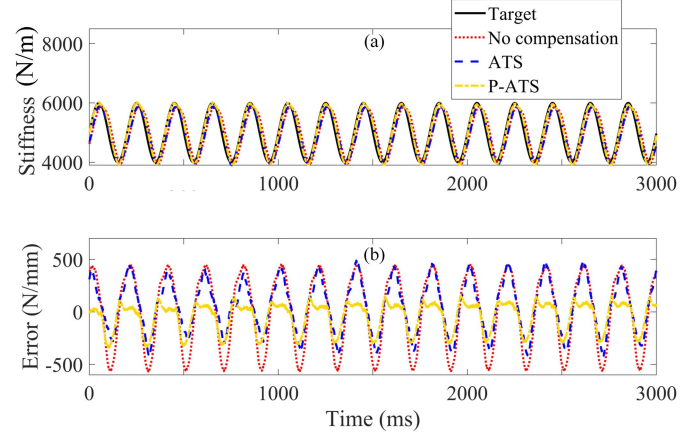


Fig. 16. Real-world experimental results of variable stiffness tracking. (a) Stiffness tracking. (b) Tracking error.

indicate that such result is brought by the distortion in the curve.

*Remark 3:* In Experiment 3, both ATS and P-ATS compensators suffer performance losses due to the reduced sampling rate. However, based on results from Table V and Fig. 15, the P-ATS compensator is less affected. Although the ATS compensator seems to achieve a lower time delay in this experiment, the introduced severe overshoot and errors suggest a distortion in the curve, which makes the estimated time delay become meaningless. Combined with Table III, the results suggest that the ATS compensator performs even worse than the noncompensated method, indicating that the ATS compensator applies adverse effects to control performance with a reduced sampling rate. In comparison, the P-ATS compensator can maintain its performance and still contribute to delay and error compensation under such conditions. The results from all three experiments suggest that the proposed method can be applied to effectively reduce both the time delay and tracking error in SEA stiffness tracking. Although the application of the ATS compensator also aids in considerable improvements in control performance, it also has adverse effects, such as instability and large overshoot. Moreover, the inability to work under conditions of low sampling rate can limit its practical applications. The collision experiment indicates a more significant superiority of the proposed P-ATS-based method by considering the external force estimation. This is due to the parallel mechanism, which saves more computational resources for parameter optimization. Combined with the WSA method, parameters with better fitness values can be located. The provided evaluation criterion also enhances the output parameter quality and system stability.

#### E. Real-World Experiment

Fig. 16 shows the results of variable stiffness tracking under a virtual constant external force. The collision experimental results are presented in Figs. 17 and 18. The details are summarized in Tables VI and VII, respectively.

It can be observed from Fig. 16 that the P-ATS compensator improves the tracking performance compared to the compar-

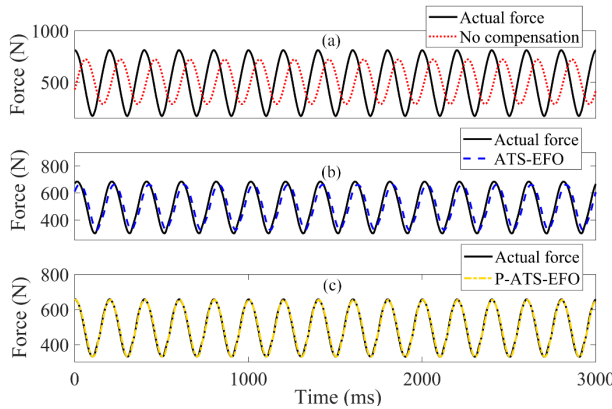


Fig. 17. Real-world experimental results of external force estimation. (a) Traditional EFO. (b) ATS-EFO; estimation error. (c) P-ATS-EFO.

TABLE VI  
REAL-WORLD VARIABLE STIFFNESS TRACKING RESULTS

Method	$\tau_d^{10}$ [ms]	$\tau_d^{30}$ [ms]	$e_{dmax}$ [mm]	$e_d$ [mm]	$v_d$	$e_{kmax}$ [N/m]	$e_k$ [N/m]
NC	21	20	5.2	2.4	---	567.2	311.7
ATS	13	13	4.8	1.9	7.7	488.1	216.5
P-ATS	2	-1	2.1	1.0	1.6	340.9	112.3

\*NC: non-compensated method. Negative value indicates a phase advance.

TABLE VII  
REAL-WORLD COLLISION RESULTS

Method	$\tau_f^{10}$ [ms]	$\tau_f^{30}$ [ms]	$e_{fmax}$ [N]	$e_f$ [N]	$v_f$	$e_{kmax}$ [N/m]	$e_k$ [N/m]
NC	64	63	445.3	275.8	---	7425.1	3316.7
ATS	16	15	80.62	48.3	0.09	2730.5	1169.2
P-ATS	1	2	17.8	6.6	0.05	880.4	399.9

\*NC: non-compensated method. Negative value indicates a phase advance.

ative methods. Results from Table VI indicate that, compared with the ATS-based method, the P-ATS-based method achieves 84.6% (from 13 to 2 ms) and 48.1% (from 216.5 to 112.3 N/m) improvements on the time delay in the short term and stiffness tracking error, respectively.

From Fig. 17, we observe that the P-ATS-EFO outperforms its competitors. The actual forces obtained by using different methods are not the same. This is because, although the experimental setup remains the same in each test, the contact force is not guaranteed due to different control performance. However, the results from Fig. 18 and Table VII indicate the SEA performances in maintaining the stiffness under the same disturbances of external force. The P-ATS-based method aids in reducing 93.8% (from 16 to 1 ms) of the time delay and 86.3% (from 48.3 to 6.6 N) of the estimation error for the EFO, resulting in a 65.8% (from 1169.2 to 399.9 N/m) improvement on stiffness tracking error.

*Remark 4:* The results obtained by real-world experiments via the experimental platform are consistent with that of the simulation experiments. Compared with simulation experiments, the results from real-world experiments indicate better performance. This is due to the preset initial parameters that

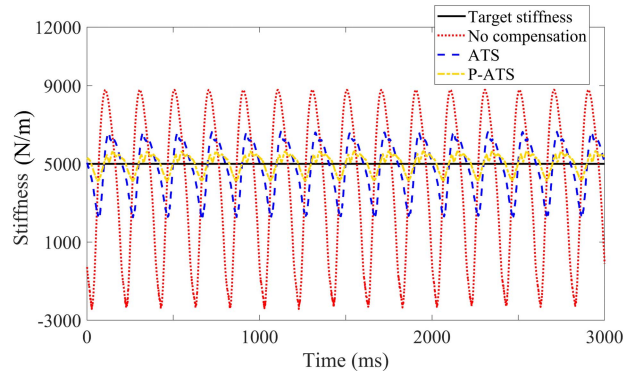


Fig. 18. Real-world experimental results of the collision experiment.

allow a faster convergence. Moreover, we observe that the P-ATS compensator achieves the maximum improvements compared to the other methods. The reason can be that the WSA algorithm gains more benefits from better initial values due to its optimization mechanism. As a result, the proposed method shows a better performance for SEA stiffness tracking in terms of time delay and tracking error, thus providing a potential solution for safe human–robot interaction.

## V. CONCLUSION

This article proposed a fast-response admittance control method for hydraulic SEAs to realize safe human–robot collaboration. A position-sourced admittance control scheme is first developed, in which an EFO is introduced to estimate the external force. However, the control performance suffers from both time delays and tracking errors due to inaccurate actuator response and external force estimation. A P-ATS compensator is, therefore, proposed and applied to both the SEA position controller and EFO to achieve high-performance stiffness tracking. The P-ATS compensator is a modification of the ATS compensator, in which a unique parallel mechanism is developed to enhance its performance. In addition, we adopt the WSA method to improve the searching ability, and the quality of the updated parameters can be guaranteed by a provided evaluation criterion. Simulation and real-world experiments were conducted to verify the effectiveness of the proposed method.

The results suggest that, compared with the noncompensated and ATS-based method, the proposed methods can achieve better performance in terms of both time delay and tracking error. We conclude that: 1) the parallel mechanism enables the P-ATS compensator to save more computational resources in parameter optimization; 2) combined with the WSA method, parameters with lower fitness values are located which leads to higher control performance; and 3) the proposed evaluation criterion aids in improving the quality of the updated parameters and avoiding inappropriate tuning. Such improvements also allow the proposed method to maintain its performance with a reduced sampling rate, which facilitates its practical application. All results suggest that the proposed method can realize high-performance stiffness rendering for SEAs, therefore demonstrating a potential solution for ensuring safe

human–robot collaboration. However, the rejection of random disturbances, such as sensor noise and inaccurate kinematics, remains to be discussed. In the future, we plan to address this problem and apply the proposed method to further collaboration task that involves interaction with human to test its performance.

## REFERENCES

- [1] S. M. M. Rahman, “A novel variable impedance compact compliant series elastic actuator: Analysis of design, dynamics, materials and manufacturing,” *Appl. Mech. Mater.*, vol. 245, pp. 99–106, Dec. 2012.
- [2] G. Adamson, L. Wang, and M. Holm, “The state of the art of cloud manufacturing and future trends,” in *Proc. Syst. Micro Nano Technol. Sustain. Manuf. (MSEC)*, vol. 2, Jun. 2013, pp. 1–9.
- [3] V. Villani, F. Pini, F. Leali, and C. Secchi, “Survey on human–robot collaboration in industrial settings: Safety, intuitive interfaces and applications,” *Mechatronics*, vol. 55, pp. 248–266, Nov. 2018.
- [4] S. Ganjefar, S. Rezaei, and F. Hashemzadeh, “Position and force tracking in nonlinear teleoperation systems with sandwich linearity in actuators and time-varying delay,” *Mech. Syst. Signal Process.*, vol. 86, pp. 308–324, Mar. 2017.
- [5] F. Sergi and M. K. O’Malley, “On the stability and accuracy of high stiffness rendering in non-backdrivable actuators through series elasticity,” *Mechatronics*, vol. 26, pp. 64–75, Mar. 2015.
- [6] L. U. Odhner, R. R. Ma, and A. M. Dollar, “Open-loop precision grasping with underactuated hands inspired by a human manipulation strategy,” *IEEE Trans. Autom. Sci. Eng.*, vol. 10, no. 3, pp. 625–633, Jul. 2013.
- [7] Y. Fu, J. Luo, D. Ren, H. Zhou, X. Li, and S. Zhang, “Research on impedance control based on force servo for single leg of hydraulic legged robot,” in *Proc. IEEE Int. Conf. Mechatronics Autom.*, Aug. 2017, pp. 1591–1596.
- [8] A. Calanca, R. Muradore, and P. Fiorini, “Impedance control of series elastic actuators: Passivity and acceleration-based control,” *Mechatronics*, vol. 47, pp. 37–48, Nov. 2017.
- [9] A. Calanca and P. Fiorini, “Impedance control of series elastic actuators based on well-defined force dynamics,” *Robot. Auto. Syst.*, vol. 96, pp. 81–92, Oct. 2017.
- [10] Y. Zhao, N. Paine, S. J. Jorgensen, and L. Sentis, “Impedance control and performance measure of series elastic actuators,” *IEEE Trans. Ind. Electron.*, vol. 65, no. 3, pp. 2817–2827, Mar. 2018.
- [11] V. Azimi, S. Abolfazl Fakoorian, T. Tien Nguyen, and D. Simon, “Robust adaptive impedance control with application to a transfemoral prosthesis and test robot,” *J. Dyn. Syst., Meas., Control*, vol. 140, no. 12, Dec. 2018.
- [12] K. Haninger, J. Lu, and M. Tomizuka, “Robust impedance control with applications to a series-elastic actuated system,” in *Proc. IEEE/RSJ Int. Conf. Intell. Robots Syst. (IROS)*, Oct. 2016, pp. 5367–5372.
- [13] A. Calanca, R. Muradore, and P. Fiorini, “A review of algorithms for compliant control of stiff and fixed-compliance robots,” *IEEE/ASME Trans. Mechatronics*, vol. 21, no. 2, pp. 613–624, Apr. 2016.
- [14] Y. Park, N. Paine, and S. Oh, “Development of force observer in series elastic actuator for dynamic control,” *IEEE Trans. Ind. Electron.*, vol. 65, no. 3, pp. 2398–2407, Mar. 2018.
- [15] E. Sarıyıldız, G. Chen, and H. Yu, “An acceleration-based robust motion controller design for a novel series elastic actuator,” *IEEE Trans. Ind. Electron.*, vol. 63, no. 3, pp. 1900–1910, Mar. 2016.
- [16] H. Dallali, P. Kormushev, N. G. Tsagarakis, and D. G. Caldwell, “Can active impedance protect robots from landing impact?” in *Proc. IEEE-RAS Int. Conf. Humanoid Robots*, Nov. 2014, pp. 1022–1027.
- [17] X. Li, Y. Pan, G. Chen, and H. Yu, “Continuous tracking control for a compliant actuator with two-stage stiffness,” *IEEE Trans. Autom. Sci. Eng.*, vol. 15, no. 1, pp. 57–66, Jan. 2018.
- [18] V. Chawda and G. Niemeyer, “Toward torque control of a KUKA LBR IIWA for physical human–robot interaction,” in *Proc. IEEE/RSJ Int. Conf. Intell. Robots Syst. (IROS)*, Sep. 2017, pp. 6387–6392.
- [19] A. D. Wilson, J. A. Schultz, A. R. Ansari, and T. D. Murphrey, “Dynamic task execution using active parameter identification with the Baxter research robot,” *IEEE Trans. Autom. Sci. Eng.*, vol. 14, no. 1, pp. 391–397, Jan. 2017.
- [20] M. Bianchi *et al.*, “Design of a series elastic transmission for hand exoskeletons,” *Mechatronics*, vol. 51, pp. 8–18, May 2018.
- [21] S. Kim and J. Bae, “Force-mode control of rotary series elastic actuators in a lower extremity exoskeleton using model-inverse time delay control,” *IEEE/ASME Trans. Mechatronics*, vol. 22, no. 3, pp. 1392–1400, Jun. 2017.
- [22] M. C. Yildirim, A. T. Kansizoglu, P. Sendur, and B. Ugurlu, “High power series elastic actuator development for torque-controlled exoskeletons,” in *Proc. 4th Int. Symp. Wearable Robot. (WeRob)*, Oct. 2019, pp. 70–74.
- [23] E. Bolivar, S. Rezaeza, T. Summers, and R. D. Gregg, “Robust optimal design of energy efficient series elastic actuators: Application to a powered prosthetic ankle,” in *Proc. IEEE 16th Int. Conf. Rehabil. Robot.*, Jun. 2019, pp. 740–747.
- [24] L. Liu, S. Leonhardt, C. Ngo, and B. J. E. Misgeld, “Impedance-controlled variable stiffness actuator for lower limb robot applications,” *IEEE Trans. Autom. Sci. Eng.*, vol. 17, no. 2, pp. 991–1004, Apr. 2020.
- [25] S. Yoo, W. Lee, and W. K. Chung, “Impedance control of hydraulic actuation systems with inherent backdrivability,” *IEEE/ASME Trans. Mechatronics*, vol. 24, no. 5, pp. 1921–1930, Oct. 2019.
- [26] H. Zhong, X. Li, and L. Gao, “Adaptive delay compensation for admittance control of hydraulic series elastic actuator,” in *Proc. IEEE 16th Int. Conf. Autom. Sci. Eng.*, Aug. 2020, pp. 384–389.
- [27] P. Mustalahti and J. Mattila, “Impedance control of hydraulic series elastic actuator with a model-based control design,” in *Proc. IEEE/ASME Int. Conf. Adv. Intell. Mechatronics*, Jul. 2020, pp. 966–971.
- [28] S. Yoo, J. Lee, J. Choi, G. Chung, and W. K. Chung, “Development of rotary hydro-elastic actuator with robust internal-loop-compensator-based torque control and cross-parallel connection spring,” *Mechatronics*, vol. 43, pp. 112–123, May 2017.
- [29] A. B. Zoss, H. Kazerooni, and A. Chu, “Biomechanical design of the berkeley lower extremity exoskeleton (BLEEX),” *IEEE/ASME Trans. Mechatronics*, vol. 11, no. 2, pp. 128–138, Apr. 2006.
- [30] A. Otten, C. Voort, A. Stienen, R. Aarts, E. van Asseldonk, and H. van der Kooij, “LIMPACT: A hydraulically powered self-aligning upper limb exoskeleton,” *IEEE/ASME Trans. Mechatronics*, vol. 20, no. 5, pp. 2285–2298, Oct. 2015.
- [31] N. L. Tagliamonte, D. Accoto, and E. Guglielmelli, “Rendering viscoelasticity with series elastic actuators using cascade control,” in *Proc. IEEE Int. Conf. Robot. Autom.*, May 2014, pp. 2424–2429.
- [32] M. Focchi *et al.*, “Robot impedance control and passivity analysis with inner torque and velocity feedback loops,” *Control Theory Technol.*, vol. 14, no. 2, pp. 97–112, May 2016.
- [33] Z. Chu, J. W. Luo, and Y. L. Fu, “Variable stiffness control and implementation of hydraulic sea based on virtual spring leg,” in *Proc. IEEE Int. Conf. Mechatron. Autom.*, Aug. 2016, pp. 677–682.
- [34] N. L. Tagliamonte and D. Accoto, “Passivity constraints for the impedance control of series elastic actuators,” *Proc. Inst. Mech. Eng. I, J. Syst. Control Eng.*, vol. 228, no. 3, pp. 138–153, Mar. 2014.
- [35] G. A. Pratt, P. Willisson, C. Bolton, and A. Hofman, “Late motor processing in low-impedance robots: Impedance control of series-elastic actuators,” in *Proc. Amer. Control Conf.*, Jun./Jul. 2004, pp. 3245–3251.
- [36] D. W. Robinson and G. A. Pratt, “Force controllable hydro-elastic actuator,” in *Proc. IEEE Int. Conf. Robo. Auto.*, Apr. 2000, pp. 1321–1327.
- [37] H. Vallery, R. Ekkelenkamp, H. van der Kooij, and M. Buss, “Passive and accurate torque control of series elastic actuators,” in *Proc. IEEE/RSJ Int. Conf. Intell. Robots Syst.*, Oct./Nov. 2007, pp. 3534–3538.
- [38] G. Wyeth, “Demonstrating the safety and performance of a velocity sourced series elastic actuator,” in *Proc. IEEE Int. Conf. Robot. Autom.*, May 2008, pp. 3642–3647.
- [39] N. Banka, W. T. Piaskowy, J. Garbini, and S. Devasia, “Iterative machine learning for precision trajectory tracking with series elastic actuators,” in *Proc. IEEE Int. Workshop Adv. Motion Control*, Mar. 2018, pp. 234–239.
- [40] J. S. Mehling, J. Holley, and M. K. O’Malley, “Leveraging disturbance observer based torque control for improved impedance rendering with series elastic actuators,” in *Proc. IEEE/RSJ Int. Conf. Intell. Robots Syst. (IROS)*, Sep./Oct. 2015, pp. 1646–1651.
- [41] J. Yang, C. Hu, Y. Zhu, Z. Wang, and M. Zhang, “Experimental investigation of shaping disturbance observer design for motion control of precision mechatronic stages with resonances,” *Mech. Syst. Signal Process.*, vol. 92, pp. 334–348, Aug. 2017.
- [42] N. Paine *et al.*, “Actuator control for the NASA-JSC Valkyrie humanoid robot: A decoupled dynamics approach for torque control of series elastic robots,” *J. Field Robot.*, vol. 32, no. 3, pp. 378–396, May 2015.
- [43] S. Oh and K. Kong, “High-precision robust force control of a series elastic actuator,” *IEEE/ASME Trans. Mechatronics*, vol. 22, no. 1, pp. 71–80, Feb. 2017.

- [44] F. Parietti, G. Baud-Bovy, E. Gatti, R. Riener, L. Guzzella, and H. Vallery, "Series viscoelastic actuators can match human force perception," *IEEE/ASME Trans. Mechatronics*, vol. 16, no. 5, pp. 853–860, Oct. 2011.
- [45] A. Colomé, D. Pardo, G. Alenya, and C. Torras, "External force estimation during compliant robot manipulation," in *Proc. IEEE Int. Conf. Robot. Autom.*, May 2013, pp. 3535–3540.
- [46] Y. Chae, R. Rabiee, A. Dursun, and C.-Y. Kim, "Real-time force control for servo-hydraulic actuator systems using adaptive time series compensator and compliance springs," *Earthq. Eng. Struct. Dyn.*, vol. 47, no. 4, pp. 854–871, Apr. 2018.
- [47] B. M. Phillips and B. F. Spencer, "Model-based feedforward-feedback actuator control for real-time hybrid simulation," *J. Struct. Eng.*, vol. 139, no. 7, pp. 1205–1214, Jul. 2013.
- [48] M. Souzanchi-K, A. Arab, M.-R. Akbarzadeh-T, and M. M. Fateh, "Robust impedance control of uncertain mobile manipulators using time-delay compensation," *IEEE Trans. Control Syst. Technol.*, vol. 26, no. 6, pp. 1942–1953, Nov. 2018.
- [49] Y. Zhao and L. Sentis, "Passivity of time-delayed whole-body operational space control with series elastic actuation," in *Proc. IEEE-RAS 16th Int. Conf. Humanoid Robots (Humanoids)*, Nov. 2016, pp. 1290–1297.
- [50] H. Yu, S. Huang, G. Chen, Y. Pan, and Z. Guo, "Human–robot interaction control of rehabilitation robots with series elastic actuators," *IEEE Trans. Robot.*, vol. 31, no. 5, pp. 1089–1100, Oct. 2015.
- [51] Y. Chae, K. Kazemibidokhti, and J. M. Ricles, "Adaptive time series compensator for delay compensation of servo-hydraulic actuator systems for real-time hybrid simulation," *Earthq. Eng. Struct. Dyn.*, vol. 42, no. 11, pp. 1697–1715, Sep. 2013.
- [52] D. Budolak and P. Ben-Tzvi, "Series elastic actuation for improved transparency in time delayed haptic teleoperation," *Mechatronics*, vol. 63, Nov. 2019, Art. no. 102278.
- [53] H. Zhong, P. Li, L. Gao, and X. Li, "Low-delay admittance control of hydraulic series elastic actuator for safe human–robot collaboration," *Procedia Manuf.*, vol. 48, pp. 147–153, 2020.
- [54] H. Zhong, X. Li, L. Gao, and H. Dong, "Position control of hydraulic series elastic actuator with parameter self-optimization," in *Proc. IEEE 4th Int. Conf. Adv. Robot. Mechatronics*, Jul. 2019, pp. 42–46.
- [55] B. Zeng, X. Li, L. Gao, Y. Zhang, and H. Dong, "Whale swarm algorithm with the mechanism of identifying and escaping from extreme points for multimodal function optimization," *Neural Comput. Appl.*, vol. 32, no. 9, pp. 5071–5091, May 2020.
- [56] H. Zhong, C. Hu, X. Li, L. Gao, B. Zeng, and H. Dong, "Kinematic calibration method for a two-segment hydraulic leg based on an improved whale swarm algorithm," *Robot. Comput.-Integr. Manuf.*, vol. 59, pp. 361–372, Oct. 2019.
- [57] R. Ettema, R. Arndt, P. Roberts, and T. Wahl, "Hydraulic modeling: Concepts and practice," *Manuals Rep. Eng. Pract.*, Amer. Soc. Civil Eng., Reston, VA, USA, Tech. Rep. 97, 2000, pp. 1–390.
- [58] N. Yu, W. Zou, and Y. Sun, "Passivity guaranteed stiffness control with multiple frequency band specifications for a cable-driven series elastic actuator," *Mech. Syst. Signal Process.*, vol. 117, pp. 709–722, Feb. 2019.



**Haoran Zhong** (Student Member, IEEE) received the B.S. degree from the East China University of Science and Technology (ECUST), Shanghai, China, in 2014. He is currently pursuing the Ph.D. degree with the State Key Laboratory of Digital Manufacturing Equipment and Technology, School of Mechanical Science and Engineering, Huazhong University of Science and Technology (HUST), Wuhan, China.

His current research interests include humanoid robots, compliant control, and intelligent algorithms.



**Xinyu Li** (Member, IEEE) received the Ph.D. degree in industrial engineering from the Huazhong University of Science and Technology (HUST), Wuhan, China, in 2009.

He is currently a Professor with the Department of Industrial and Manufacturing Systems Engineering, State Key Laboratory of Digital Manufacturing Equipment and Technology, School of Mechanical Science and Engineering, HUST. He has authored more than 80 refereed articles. His research interests include intelligent algorithms, big data, and machine learning.



**Liang Gao** (Senior Member, IEEE) received the Ph.D. degree in mechatronic engineering from the Huazhong University of Science and Technology (HUST), Wuhan, China, in 2002.

He is currently a Professor with the Department of Industrial and Manufacturing System Engineering, State Key Laboratory of Digital Manufacturing Equipment and Technology, School of Mechanical Science and Engineering, HUST. He has authored more than 170 refereed articles. His research interests include operations research and optimization, big data, and machine learning.



**Congbo Li** (Senior Member, IEEE) received the Ph.D. degree in industrial engineering from Chongqing University, Chongqing, China, in 2009.

He is currently a Professor of mechanical engineering with Chongqing University. His research interests include modeling and optimization control, energy-efficient manufacturing. His work has resulted in one book, and over 100 journal and conference proceeding articles.

Prof. Li is currently serving as a Co-Chair for the IEEE RAS TC on Sustainable Production Automation and an Associate Editor for the IEEE TRANSACTIONS ON AUTOMATION SCIENCE AND ENGINEERING.